Available online at www.sciencedirect.com
SCIENCE DIRECT®
International Journal of Refractory Metals & Hard Materials 24 (2006) 89–100
International Journal of REFRACTORY METALS & HARD MATERIALS
www.elsevier.com/locate/ijrmhm

Modeling the relationship between microstructural features and the strength of WC–Co composites

Chang-Soo Kim [a], Ted R. Massa [b], Gregory S. Rohrer [a,*]

[a] *Department of Materials Science and Engineering, Carnegie Institute of Technology, 5000 Forbes Avenue, Carnegie Mellon University, Pittsburgh, PA 15213, USA*

[b] *Kennametal Incorporated, Corporate Technology, 1600 Technology way, P.O. Box 231, Latrobe, PA 15650, USA*

Received 11 November 2004; accepted 12 April 2005

Abstract

A two-dimensional finite element method (FEM) was used to predict the stress–strain distributions and the fracture strengths of WC–Co composites with carbide grain sizes from 1.4 to 5.3 μm and carbide volume fractions from 0.7 to 0.9. Stress–strain distributions were calculated in plane sections of microstructures mapped by orientation imaging microscopy. An effective fracture energy was set so that the measured strength of each material was reproduced by the simulation. This model was then used to simulate the properties of hypothetical microstructures to investigate the influence of independent variations in microstructural characteristics on strength. The results indicate that composites with minimum contiguity, containing highly angular, and equiaxed carbide grains with a narrow size distribution should have the maximum strength. Of these parameters, contiguity is the most influential.

Keywords: WC–Co composites; Microstructure; Fracture strength; Stress; Finite element method (FEM)

1. Introduction

Tungsten carbide cobalt (WC–Co) composites (usually referred to as cemented carbides or sintered carbides) are common hard materials. The combination of hard carbides (WC, hexagonal, $\bar{6}m2$) and a ductile binder (Co, hexagonal, 6/*mmm*) produces outstanding mechanical properties that make these materials commercially useful in machining, mining, metal cutting, metal forming, construction, and other applications [1,2]. Like many other engineered materials, the mechanical properties of WC–Co composites are strongly influenced by their microstructures. The effects of the grain size and volume fraction of the carbide phase on the hardness and fracture toughness are relatively well understood [3]. However, because some microstructural characteristics are strongly coupled, their independent effects on properties are not known. For example, recent measurements have illustrated that the contiguity of the carbide skeleton is linearly related to the carbide volume fraction and independent of grain size [4]. Therefore, it is difficult to experimentally study how one of these characteristics independently affects the properties of the composite.

The purpose of this work is to understand how the microstructural characteristics of WC–Co composites (contiguity, angularity, aspect ratio, and grain size distribution) affect their responses to mechanical and/or thermal loads. By simulating the responses of hypothetical microstructures, the effects of microstructural characteristics that are usually linked in real materials, such as the carbide volume fraction and the contiguity, can be independently evaluated. To numerically approximate the stress–strain distributions and fracture strength of

* Corresponding author. Tel.: +1 412 268 2696; fax: +1 412 268 3113.
E-mail address: gr20@andrew.cmu.edu (G.S. Rohrer).
URL: www.materials.cmu.edu/rohrer (G.S. Rohrer).

0263-4368/$ - see front matter © 2005 Elsevier Ltd. All rights reserved.
doi:10.1016/j.ijrmhm.2005.04.011

these materials, a two-dimensional object-oriented finite element approach (OOF) was used [5–7]. Based on the finite element method (FEM), OOF is designed to approximate solutions in stress–strain states of microstructures under mechanical and/or thermal loads. Its primary merit is its ability to model the stress–strain fields of complicated microstructures consisting of hundreds of grains. Previously, FEM models of WC–Co composites were limited to relatively localized areas of the microstructure [8,9]. Another advantage of the OOF package is that anisotropic materials specific properties (crystallographic orientations, stiffness, and coefficients of thermal expansion) of individual crystals are easily incorporated and used for the calculation of the internal stress and strain.

The OOF model can also be used to simulate fracture. Here, an effective fracture energy has been set so that the measured strengths of real materials are reproduced by simulations that use their microstructures as input. With this effective fracture energy, the stress distributions, elastic energy density distributions, and the strengths of hypothetical microstructures were calculated. These microstructures were created to independently vary particular microstructural characteristics (the contiguity, angularity, aspect ratio, or grain size distribution) while keeping the others as constant as possible, so that each parameter's influence on the strength could be independently determined. The methods used to characterize the microstructures of real WC–Co composites are described in the next section. In Section 3 the simulation method is briefly described. The results for the real and hypothetical WC–Co microstructures are then presented and discussed in Sections 4 and 5, respectively. The conclusions are stated in Section 6.

2. Experimental

Four WC–Co specimens with different microstructural characteristics (grades A through D) were provided by Kennametal Inc., Latrobe, PA, USA. The samples were consolidated via liquid phase sintering for approximately 45 min at temperatures in the range of 1400 °C to 1600 °C. These specimens contained no intentional alloying additions and are referred to as straight WC–Co grades. Based on measurements of each sample's magnetic saturation, it was concluded that all of the materials had approximately the same amount of W and C dissolved in the binder. These particular materials were selected because they span a range of grain size and carbide volume fraction (see Table 1). The effect of grain size on strength can be demonstrated by comparing grades A and B (different grain sizes with the same carbide volume fraction), and effect of carbide volume fraction on strength can be demonstrated by comparing grades B, C, and D, which have different carbide volume fractions, but similar grain sizes. The microstructural features in Table 1 were determined from the analysis of atomic force microscope and electron backscattered diffraction maps, as previously described [4].

Table 1
Measured microstructural features and transverse rupture strength (TRS) for specimen grades A–D

Grade	$\bar{d}$ (μm)	λ (μm)	f_c	C	TRS (GPa)
A	5.31 (3.19)	1.72 (1.35)	0.89	0.60	1.94 (0.05)
B	1.65 (0.97)	0.53 (0.39)	0.89	0.59	3.29 (0.13)
C	1.41 (0.90)	0.63 (0.48)	0.82	0.50	2.84 (N/A)
D	1.40 (0.88)	0.96 (0.81)	0.69	0.35	2.57 (N/A)

$\bar{d}$ is the average WC diameter, λ is the binder mean free path, f_c, is the WC volume fraction, C is the contiguity, and TRS is the transverse rupture strength, respectively. The values in parenthesis denote standard deviations.

The microstructural characteristics were evaluated using orientation imaging microscopy (OIM, TexSEM Laboratories, Inc., UT, USA) data. Before analysis, the samples were slowly polished using a diamond abrasive and etched in Murakami's reagent (10 g potassium ferricyanide + 10 g sodium hydroxide + 100 ml distilled water) for 1 min. Orientation measurements were made at intervals of 1.0 μm (A) and 0.2 μm (B, C, and D) over total areas of 600×600 μm^2 and 180×180 μm^2, respectively, with an accelerating voltage of 20 kV, and a tilt angle of 70°. Microstructural features smaller than the resolutions of these micrographs are not accounted for in the property calculations. While the sample preparation method produced suitable diffraction patterns from the WC crystals, it was not possible to index the patterns from the Co. The orientation data were processed to remove spurious observations using the 'grain dilation clean-up' procedure in the OIM software (TexSEM Laboratories, Inc. version 3.03). Before the clean-up procedure, the crystallographic orientation of the Co phase has been fictitiously assigned so that WC/Co boundaries could be easily discriminated from WC/WC boundaries; the process also keeps the WC/Co boundaries from being distorted during the grain clean-up procedure. After clean-up, a single orientation was assigned to each carbide grain by averaging all of the orientations within a single grain that were measured with a confidence index greater than 0.2. The result is that a unique orientation can be assigned to each grain and the carbide/carbide and carbide/Co boundaries are clearly delineated, as illustrated in Fig. 1. Details of this OIM analysis have already been reported elsewhere [4,10].

The Young's modulus of each sample was measured using a Panametrics Pulse Ultrasonic test unit. The tests were conducted in accordance with ASTM procedure E494-95(2001) for measuring ultrasonic velocity in materials. The fracture strength (TRS) was measured using a three-point bend test. The dimensions for the

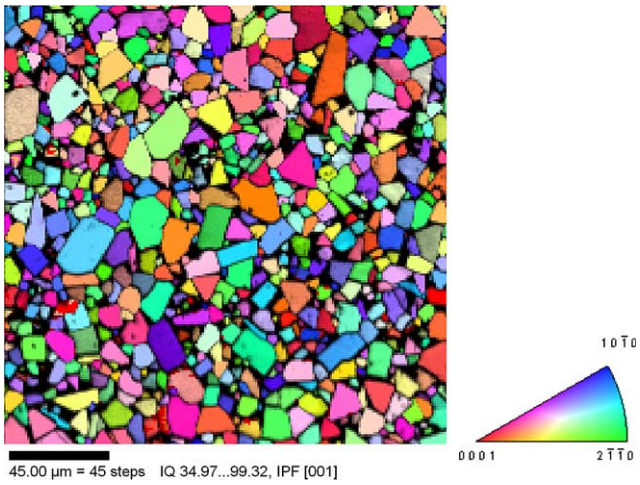

Fig. 1. An example of OIM inverse pole figure (IPF) map (from grade A). The Co orientations were not determined (black).

TRS test specimens were $5 \times 5 \times 20$ mm^3, the span of the TRS test was 14.29 mm, and, for statistical reliability, more than 15 independent TRS measurements were averaged. The fracture strengths are listed in Table 1. Here, the values in parentheses are the standard deviations in each grade. The standard deviations of the fracture strength range from 3% to 7% of the measured strengths.

3. Simulation method

3.1. Real microstructures

Three independent sections, each containing from 600 to 900 WC grains, were used for the calculations. Subsets of the much larger OIM maps were used to create the model structures. Areas in the OIM map corresponding to WC were assigned orientations from the OIM data and corresponding anisotropic elastic and thermal characteristics. Because the Co orientations were not recorded, it was assumed to be isotropic, pure, and modeled with a single elastic modulus and Poisson's ratio. Table 2 shows the elastic constants and the coefficient of thermal expansion (CTE) of the WC and Co phases that were used in the present calculations [11–13]. In all of the calculations presented here, we have assumed that the CTE of the WC and Co phases are constant at all temperatures. After orientations and properties were assigned to each area in the planar sections, the microstructures were discretized using ~180,000–210,000 triangular finite elements.

The OOF software package (OOF, version 1.1.17, National Institute of Standards and Technology, Gaithersburg, MD) was used to calculate the responses of the discretized microstructures to mechanical and thermal loads. In these simulations, the stress and strain at each point in the microstructure is calculated. All of the simulations in this work were carried out under the plane-stress condition with fixed boundary conditions (this means that the surfaces of the model perpendicular to the direction of elongation are fixed during the calculation) and the results are averages from three sections loaded in both the x- and y-directions during independent tests.

Table 2
(Panel a) Elastic constants and (Panel b) coefficients of thermal expansion of the WC and Co phases [11–13]

	WC	Co
Panel a		
C_{11} (GPa)	720	
C_{33} (GPa)	972	
C_{44} (GPa)	328	
C_{12} (GPa)	254	
C_{13} (GPa)	267	
E (GPa)	714	211
ν	0.19	0.31
Panel b		
α_{11} (/K)	5.2e−6	
α_{33} (/K)	7.3e−6	
α (/K)		1.4e−5

C_{11}–C_{13} are the stiffness of WC, E is the bulk Young's modulus, ν is the Poisson's ratio of WC and Co, α_{11} and α_{33} are the anisotropic coefficients of thermal expansion of WC, and α is the isotropic coefficient of thermal expansion of Co.

The fracture strength is taken as the stress at the point where the elastic energy density exceeds the critical threshold. This is based on a Griffith-like (brittle) fracture criterion [7]:

$$2\gamma\Delta L \leqslant \frac{1}{2}\sigma_{ij}\varepsilon_{ij}A \tag{1}$$

in which γ is the surface energy of the cracked interface, ΔL is the edge length, A is the area, σ_{ij} is the stress, and ε_{ij} is the strain of an element, respectively. Thus, the key to this analysis is to find the first crack initiation point as the mechanical load is incrementally increased. It should be recognized that the actual fracture process is quite complex, includes plastic deformation, and four possible fracture paths (intergranular along WC/WC boundaries, intergranular along WC/Co interfaces, transgranular in WC crystals, and transgranular in the Co) [14,15]. To simplify the situation, we assume that the fracture always initiates in the WC phase after the elastic energy surpasses a critical limit given by Eq. (1). It must also be assumed, therefore, that there is a homogeneous and sufficiently high density of crack initiation sites so that the failure always occurs at the point with the greatest strain energy. Finally, it is also assumed that the details of the various energy dissipation mechanisms during failure, including plastic processes in the Co and various initiation mechanisms, can be averaged to a single quantity that we define as the effective fracture

energy (γ). It is also assumed that this threshold value is relatively independent of the microstructural characteristics in WC/Co composites. Since this value is not known, it will be fixed so that the measured fracture strengths are reproduced by the model. With this value set appropriately, the model will then be extended to hypothetical microstructures.

3.2. Hypothetical microstructures

The same simulation approach has been applied to calculate the stress–strain distributions and fracture strengths of hypothetical WC–Co composites. Hypothetical microstructures were created either from simulations or from real microstructures of other composite materials. The methods used to generate hypothetical WC–Co microstructures are described below. From simulations of the real microstructures, it was found that as long as the crystallographic texture is random, the anisotropy of the elastic properties and the thermal load affect the absolute values of the strength, but not the trends in the strength. Therefore, fracture strengths for hypothetical microstructures were calculated using only a mechanical load and the average elastic properties of WC (bulk Young's modulus = 714 GPa and Poisson's ratio = 0.19) [11]. In each case, the results are based on averages of five independent simulations.

Hypothetical microstructures were created with the goal of changing a single microstructural characteristic, while keeping the others constant. To create microstructures with different contiguities while maintaining the carbide volume fraction, grain size, size distribution, and angularity, a Monte Carlo seeding method was used. The procedure starts by randomly selecting a grain size within the specified range, and determining the probability that it will be found in a Gaussian distribution. A second random number is then generated and compared to the probability. If the new number is less than the probability, a new grain size is selected. If it is greater, a random position is selected for the grain, then it is positioned in the microstructure, and the contiguity is calculated. If the new grain changes the contiguity so that it is closer to the target, it is preserved. If not, it is removed. In either case, the grains are selected and positioned in this fashion until the microstructure reaches the desired carbide volume fraction. With this algorithm, it is possible to control the contiguity while preserving nearly constant quantities of other microstructural features.

The hypothetical microstructures created by this Monte Carlo seeding process are based on self-similar geometric shapes and are, therefore, rather simple in comparison to real WC–Co composites. Therefore, some more complex microstructures were also created using real micrographs as starting points. Hypothetical microstructures with the same grain size and carbide volume fraction, but different contiguities, were made by randomly selecting a WC/WC boundary and reassigning these pixels to Co. After each step, the carbide fraction is calculated and compared to the target value; the procedure is stopped when the target is reached. The shortcoming of this method is that it is not feasible to create a higher contiguity microstructure than the original one; some WC/WC grain boundaries are always eliminated. Hence, the pre-determined carbide volume fraction must be smaller than the fraction in real microstructure. Furthermore, it is not possible to fully control the contiguity. Once the newly calculated carbide volume fraction is less than the pre-determined fraction, the process is stopped. Therefore, in every trial to create a hypothetical microstructure, the final contiguity cannot be fixed, and it varies within a certain range.

4. Real microstructures

To test the performance of the OOF program, the effective modulus (composite modulus) of each grade was calculated and compared to experimentally measured moduli (see Fig. 2). The error bars indicate the standard deviations in the results from the three sections (all the error bars presented in results for real and hypothetical microstructures denote the standard deviations in the computations from multiple sections). It is clear that the calculated moduli for all grades exhibit slightly lower values than the measured data. These systematic negative deviations are probably because the Co binder is not pure and, therefore, it does not have the same modulus as pure Co, which was assumed in the calculation. We can be certain that the binder in the composites

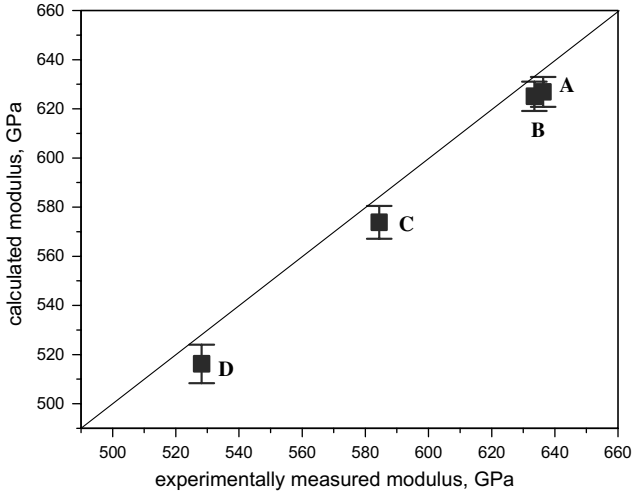

Fig. 2. Comparison of the calculated and experimentally measured modulus for each grade. Calculated moduli show systematic negative deviations. The diagonal line indicates a one-to-one correspondence between calculated and measured modulus.

contains dissolved W and C and this might increase the modulus by a small amount, which would explain the systematic difference in Fig. 2. In any case, it is worth noting that the absolute values of the errors fall in the range of only one or two percent, and are therefore not considered to be significant.

Since the effective fracture energy (γ) for the composites is not known, the fracture strength was computed as a function of assumed γ. Because the composites are sintered in the 1400–1600 °C range, a thermal load of $\Delta T = -1400$ °C was applied with plane-stress and fixed boundary conditions. Although the quenching temperature (1400 °C) is slightly higher than the solidus, quenching from lower temperatures produced essentially the same results. Since transverse rupture strength (TRS) is usually used as a measure of strength in WC–Co composites, the effective fracture energy in the carbide phase was calibrated so that the model reproduced the measured TRS values. Using the data from three simulations of each grade, the best fit value of the effective fracture energy was determined to be 49 J/m^2. Interestingly, this is consistent with the value assumed in the work of Sigl and Fischmeister, who took it to be 50 J/m^2 [15]. This value can be rationalized by assuming that the effective fracture energy in the plane-stress conditions is $G_{IC} = (K_{IC})^2/E$, where G_{IC} is the critical energy release rate, K_{IC} is the critical stress intensity factor, and E is that elastic modulus of WC. If we take the K_{IC} and E for WC to be $\sim$ 6–7 MPa$\sqrt{\text{m}}$ and 714 GPa, respectively, the fracture energy is calculated to be $\sim$50–68 J/m^2. In the case of the plane-strain condition, the effective fracture energy is $G_{IC} = (K_{IC})^2(1-\nu^2)/E$, where ν is the Poisson's ratio (0.19); this expression results in an effective fracture energy of 48–66 J/m^2.

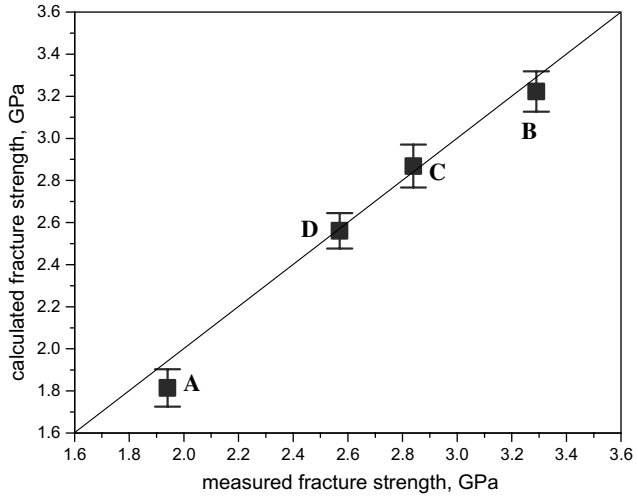

Fig. 3. Comparison of the calculated and measured fracture strength. Error bars denote the standard deviation (in sections) of the calculated fracture strength.

Using the effective fracture energy, the calculated fracture strengths are compared with measured TRS data in Fig. 3. The differences between the calculated results and the measured data are in the range of 6%. Thus, the effective fracture energy (γ) is approximately independent of the grain size and volume fraction of the carbide phase. The results indicate that strength decreases with increasing grain size and increases with increasing carbide volume fraction. It should be noted that the trends in the results are insensitive to the choice of γ. By repeating the calculations with different assumptions for γ, a linear variation in the strength was found. In other words, the ratios of the calculated strengths of the four specimens did not depend on the choice of γ.

5. Hypothetical microstructures

5.1. Contiguity

Three hypothetical microstructures with square shaped crystals, produced by the Monte Carlo seeding method, are illustrated in Fig. 4. These microstructures were designed to have different contiguities while maintaining the carbide volume fraction, grain size, grain size distribution, and angularity. The contrast levels were assigned randomly to distinguish the individual grains. The carbide volume fraction and grain edge lengths of the microstructures were set to 0.9 and 1.5, respectively, where the grain edge length is measured in arbitrary units, a.u. Because the contiguity of real WC–Co composites is 0.59 when the carbide volume fraction is 0.9 (specimen grades A and B), the contiguities of the hypothetical microstructures were set at 0.59, 0.35 and 0.02. The hypothetical microstructures were simulated using the same conditions as the real WC–Co microstructures: plane-stress and fixed boundary conditions.

The stress invariant 1 ($\sigma_{xx} + \sigma_{yy} + \sigma_{zz}$, hydrostatic stress, hereafter SI1, in units of pascal) and elastic energy density (hereafter EED, in units of a.u.) distributions for the different microstructure are shown in Fig. 4(d) through (i) with a mechanical load of 0.1% elongation along the y-direction. It is apparent that in the high contiguity microstructure, the stresses and stored energies are more concentrated in the WC phase. In the low contiguity microstructure, the Co phase breaks up the WC skeleton and prevents stresses from being dissipated in the much stiffer phase. To quantify this effect, the average stresses on each phase in five independent sections were averaged and the results are shown in Fig. 5. While the average stresses on the composites are nearly the same, the average stress ratio of the carbide to binder phase (average stress of WC/average stress of Co) increases as the contiguity increases. The contiguity effect is more obvious when we compare the calculated fracture strengths under mechanical loads in

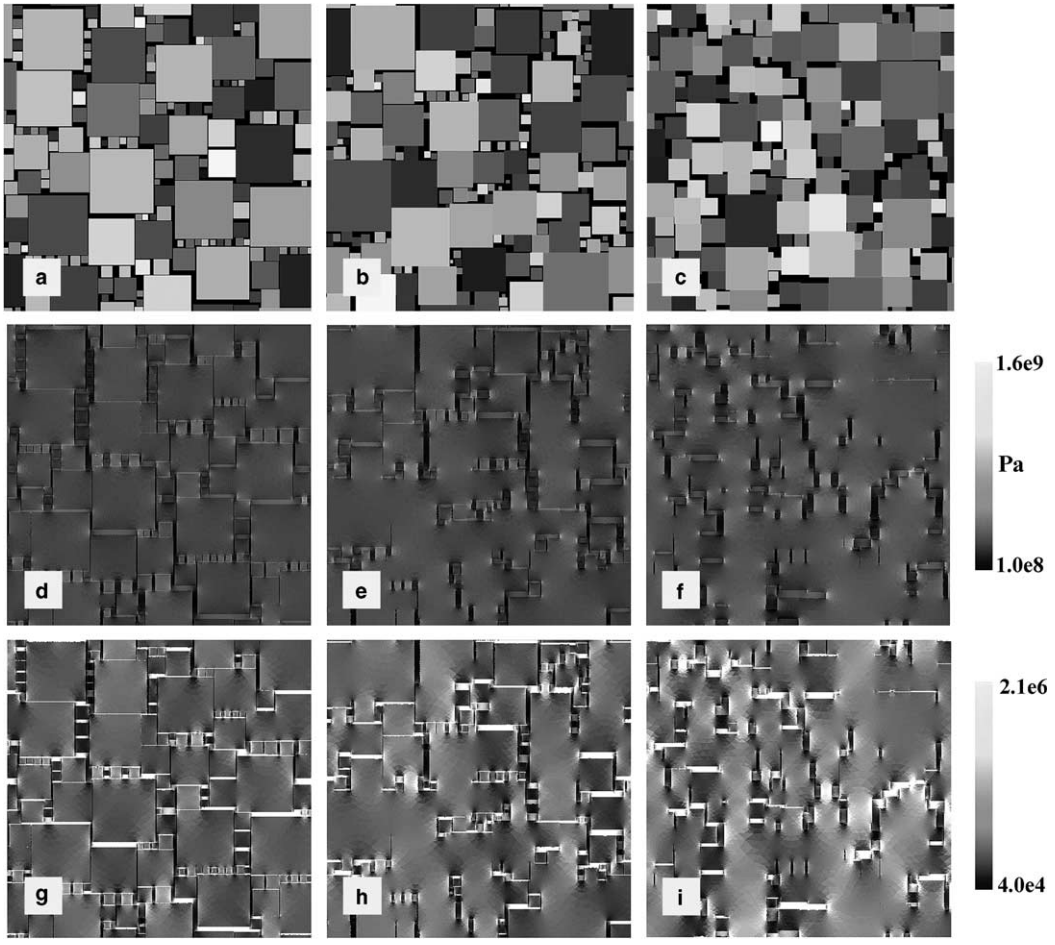

Fig. 4. Examples of hypothetical microstructures (contiguity) with their SI1 (Pa) and EED (a.u.) distributions. Simulations performed under mechanical load alone (0.1% y-elongation), fixed and plane-stress boundary conditions. (a) Low contiguity (0.02), (b) medium contiguity (0.35), (c) high contiguity (0.59) microstructures, (d)–(f) SI1 distributions (same scale) for (a)–(c) microstructures, respectively, (g)–(i) EED distributions (same scale) for (a)–(c) microstructures, respectively.

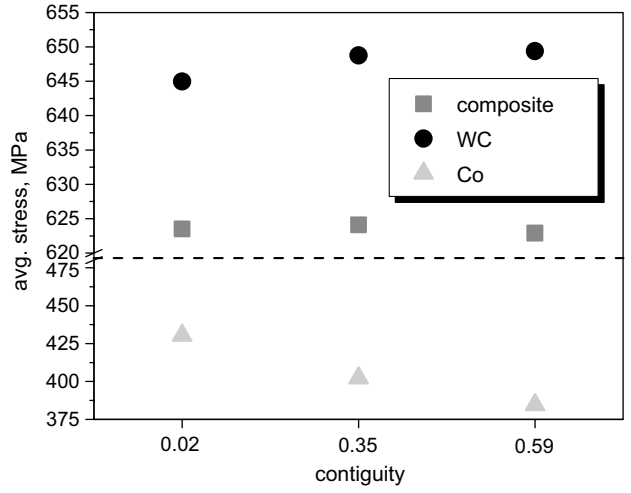

Fig. 5. Average stresses in the composites, carbide and binder phases with different contiguities (0.1% y-elongation, mechanical load alone, plane-stress and fixed boundary conditions). The average stress in the carbide phase increases as contiguity increases. Results from one section (same section shown in Fig. 4).

Fig. 6. The estimated fracture strength increases by ~7% as the contiguity decreases from 0.59 to 0.02. It should be noted that the width of grain size distributions in these microstructures decreases with the contiguity because of the Monte Carlo approach that was used to generate the hypothetical microstructures. The low contiguity microstructure has a wider distribution and the high contiguity microstructure shows a narrower distribution. The normalized standard deviations ($\sigma/\bar{d}$, standard deviation/average grain size) are 0.5, 0.7, and 0.8 with the contiguities of 0.59, 0.35, and 0.02. Since it has been found that the wide distribution has a negative effect on fracture strength (see the results of size distributions), the effects of contiguity on the strength would presumably have been larger if the hypothetical microstructures had the same grain size distribution.

To generate more realistic hypothetical microstructures, the boundary removal method was applied to OIM sections of specimen grade B ($f_c = 0.899$, $\bar{d} = 1.65$ μm, where f_c denotes the carbide volume fraction). Specimen grade B was a good starting point, since it has

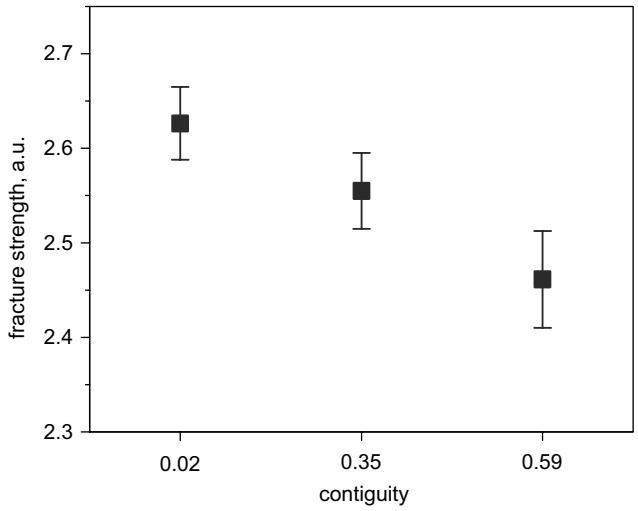

Fig. 6. Plot of the calculated fracture strength (a.u.) with different contiguities. A mechanical load was applied with plane-stress and fixed boundary conditions.

the highest contiguity. From these sections, microstructures with carbide volume fractions of approximately 0.69, analogous to specimen grade D ($f_c = 0.695$, $\bar{d} =$ 1.40 μm), were created. In other words, the hypothetical structures created from grade B have the same microstructural features as grade D, but a different contiguity. Of course, the average carbide grain sizes of the hypothetical and real grade D are different, but this can easily be corrected by changing the size of computational domains in the OOF simulations. The distributions of EED in two microstructures that have the same carbide volume fraction (0.69) but different contiguities (0.32 and 0.06) when elongated by 0.1% in the y-direction are shown in Fig. 7. For clarity, the EED distribution for the carbide phase alone is shown (Fig. 7(c) and (d)). As for the more regular microstructures illustrated in Fig. 7, the propagation of high energy density paths through the carbide skeleton is diminished in the low contiguity sample where the Co breaks up the continuous skeleton. The calculated fracture strengths are 2.53 and 2.71 GPa for the high and low contiguity microstructures, respectively. Note that for specimen grade D, the experimentally measured TRS is 2.57 GPa and the standard deviation is 0.09 GPa. While the calculated strength for the real grade D (Fig. 7(b)) is close to the measured value, the strength for the hypothetical grade D (Fig. 7 (a)) is beyond the range of the standard deviation. In tests of other structures created in the same way, the low contiguity samples always had a higher strength than their high contiguity counterparts. The reason for this is that when the contiguity is high, the load is transmitted through the carbide phase, which is stiffer. When the contiguity is low, the compliant binder carries more of the load and dissipates strain energy.

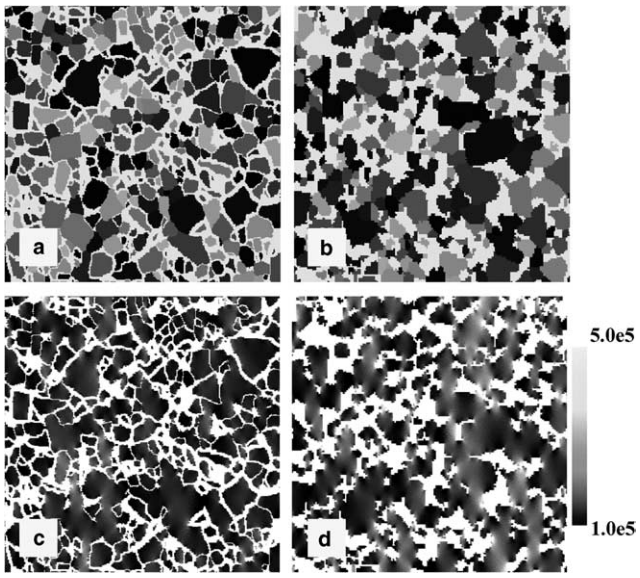

Fig. 7. Examples of hypothetical microstructures (contiguity) with their EED (a.u.) distributions. Simulations performed under a mechanical load alone (0.1% y-elongation), fixed and plane-stress boundary conditions. (a) Low contiguity (0.06) microstructure (hypothetical grade D, from real grade A), (b) high contiguity (0.32) microstructure (real grade D), (c) and (d) EED distributions (carbide phase only, same scale) for the microstructures (a) and (b), respectively.

5.2. Angularity

The effect of angularity on strength was explored using hypothetical images with completely dispersed WC particles (zero contiguity). The microstructures were generated by randomly positioning the crystals under the condition that they do not impinge. To realize such structures, it was necessary to limit the carbide volume fraction to 0.55. Fully dispersed microstructures have been selected because it is difficult to control angularity while maintaining constant finite contiguity. It is, however, already verified that low contiguity microstructures exhibit higher strengths. Thus, it can be assumed that we are testing the effect of angularity in a situation where the contiguity is constant and at a value where the strength is maximized.

Squares and circles were used as models for high and low angularity crystals, respectively (see Fig. 8(a)–(c)). Model microstructures with randomly assigned orientations and fixed orientations are illustrated in Fig. 8(a) and (b), respectively, and the distributions of stresses and elastic energy density (carbide phase only) are shown in Fig. 8(d) through (i). Under equivalent loading, samples with square shapes experience higher stresses and elastic energies than those with circular shapes. This is because the stresses and elastic energies are more easily redistributed in the microstructures containing curved interfaces. Furthermore, the results show that the microstructure made up of squares with fixed orientations

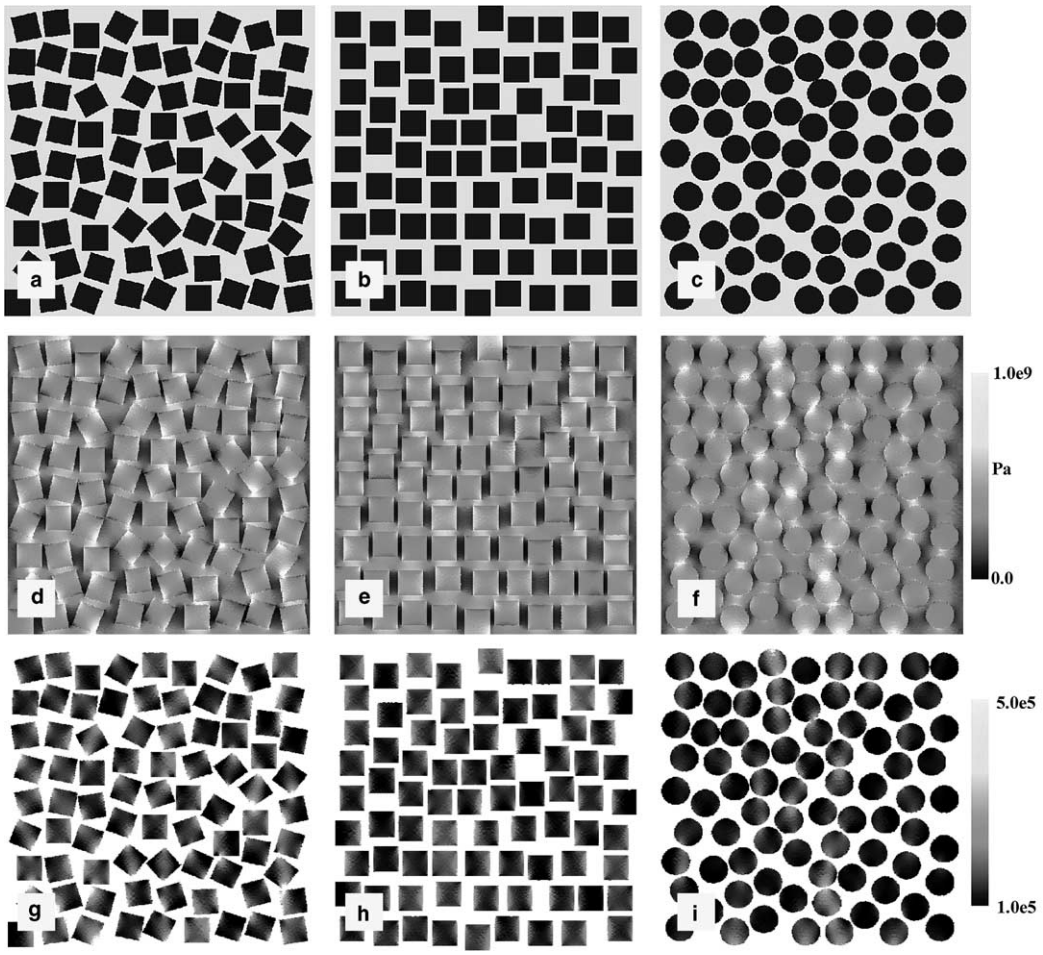

Fig. 8. Examples of hypothetical microstructures (angularity) with their SI1 (Pa) and EED (a.u.) distributions. Simulations performed under a mechanical load alone (0.1% *y*-elongation), fixed and plane-stress boundary conditions. (a) Square microstructure with random orientations (square 1), (b) square microstructure with a fixed orientation (square 2), (c) circle microstructure, (d)–(f) SI1 distributions (same scale) for square 1, square 2, and circle, respectively, (g)–(i) EED distributions (carbide only, same scale) for square 1, square 2, and circle, respectively.

(Fig. 8(b)) has lower stresses and elastic energy density in the carbide phase than the microstructures with random orientations (Fig. 8(a)). This presumably arises from differences in binder free path distributions. The binder free path distribution in Fig. 8(a) is wider than that in Fig. 8(b). This suggests that a uniform distribution of binder free paths increases the strength of the composites.

The calculated fracture strengths are plotted in Fig. 9. The data show that fracture strength increases by 3% as the shape changes from randomly oriented squares to circles. The stress ratio (average stress in WC/average stress in Co), not shown, decreases by 6%. Based on the results from the simple hypothetical microstructures discussed above, it can be concluded that the low angularity sample has an advantage over the high angularity structure in fully dispersed microstructures.

To test the effect of angularity in microstructures with realistic contiguities, hypothetical high and low angularity microstructures were created from observed micro-

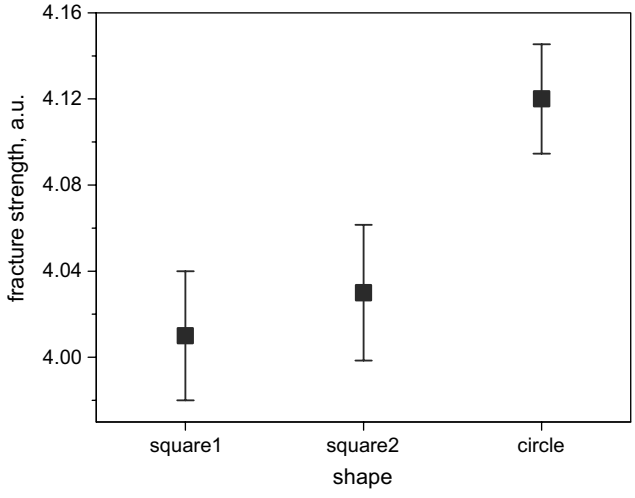

Fig. 9. Plot of the calculated fracture strength (a.u.) with different angularities (or shapes). Hypothetical microstructure with a circular shape shows a higher fracture strength.

structures. OIM data from a W–Ni–Fe alloy was used as a model for the low angularity microstructure; this microstructure contains rounded W crystals dispersed in a Ni–Fe matrix. The particle volume fraction and contiguity in this microstructure are 0.79 and 0.16, respectively. The rounded W crystals were assigned the properties of WC and the matrix was assigned the properties of Co. To create a high angularity microstructure with the same carbide volume fraction and contiguity, boundaries were removed from a microstructure observed in specimen grade B. The hypothetical microstructures and their responses to loading are illustrated in Fig. 10.

There are no obvious differences in the EED distributions for these low and high angularity microstructures. Fracture strengths were determined to be 2.81 and 2.89 GPa for the low and high angularity sample shown in Fig. 10(a) and (b), respectively. In several other sections that were tested, the calculated fracture strength in the high angularity microstructures was, on average, ~0.1 GPa higher than the low angularity structures. This modest effect is thought to be caused by the differences in the dihedral angles at junctions where Co meets a WC bicrystal. When the carbide grains are less angular, the dihedral angles where particles meet are smaller and this configuration acts as a stress concentrator when oriented properly with respect to the loading direction. The incrementally better performance of the high angularity structure contradicts the results of the zero contiguity simulations. This means that while low angularity might improve the strength of composites with a vanishingly small contiguity, is does not have the same effect at high contiguities. In commercial WC–Co composites, where the carbide faction and contiguity are relatively high, the spherical or ellipsoidal particles are expected to have a small, but detrimental effect on the strength.

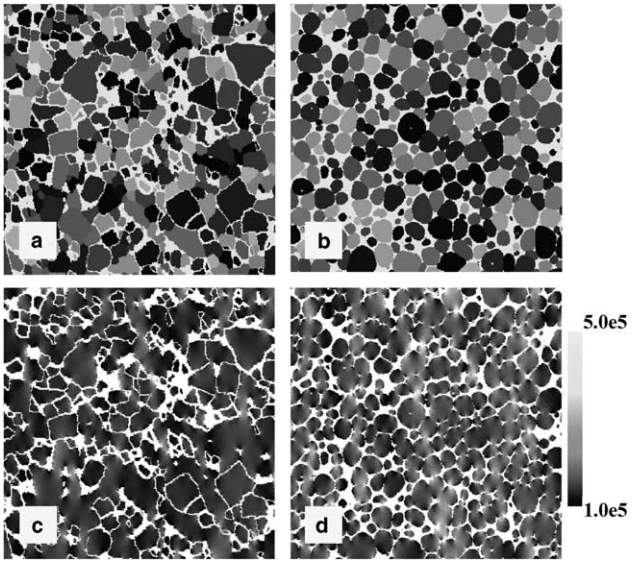

Fig. 10. Examples of hypothetical microstructures with their EED (a.u.) distributions. Simulations performed under a mechanical load alone (0.1% *y*-elongation), fixed and plane-stress boundary conditions. Input for the OOF simulation of (a) high angularity (WC/WC boundaries were selectively removed from grade A), (b) low angularity microstructures (W–Ni–Fe alloy, courtesy of A.D. Rollett, Carnegie Mellon University), (c) and (d) EED distributions (carbide only, same scale) for high and low angularity microstructures, respectively.

5.3. Aspect ratio

To test the influence of aspect ratio on the strength, fully dispersed microstructures made up of square and rectangular crystals (see Fig. 11) were created. The shapes had aspect ratios of 1:1, 1:2, and 1:4 and the carbide volume fraction was fixed at 0.55. It is clear from Fig. 11 that when the aspect ratio is large, the stress and elastic energy density exhibit a wider distribution. The stress and elastic energy are directly transmitted through elongated carbide particles that are parallel to the loading direction. Although the model structures discussed here are very simplified, they clearly show that equiaxed (aspect ratio of 1:1) shapes can provide better reinforcements than elongated (aspect ratios of 1:2 and 1:4) shapes. This is because high stresses are easily transmitted through the elongated carbide grains that are parallel to the loading direction. Reduced stresses and elastic energies were found in the carbide grains elongated perpendicular to the loading direction. In other words, in samples with high aspect ratios, the stress and elastic energy density distributions are wider than those in samples with equiaxed carbide shapes, and this is detrimental to the fracture strength of WC–Co composites. The results in Fig. 12 show that the calculated fracture strength decreases by 4% as the aspect ratio increases from 1:1 to 1:4.

5.4. Size distribution

The effect of size distributions on strength was investigated in a way that is similar to the studies of angularity and aspect ratio. The carbide shape is assumed to be square, the orientation random, and the carbide particles are fully dispersed. Again, the carbide volume fraction was fixed at 0.55 to avoid impingement of the WC particles. Examples of hypothetical microstructures with different square edge size ratios (1:1, 1:2, and 1:4) are given in Fig. 13(a)–(c). There are identical numbers of small and large crystals in these microstructures. The results show that when the size distribution is wider, the load is concentrated in the larger carbide grains. On the other hand, when the size distribution is narrower (or uniform), the stresses and elastic energies are evenly distributed, and this lead to improved strength. The calculated fracture strength (see Fig. 14) decreases by 3% as the size ratio increases from 1:1 to 1:4. Therefore, it is concluded that a homogeneous size distribution has a beneficial effect on the strength of WC–Co composites.

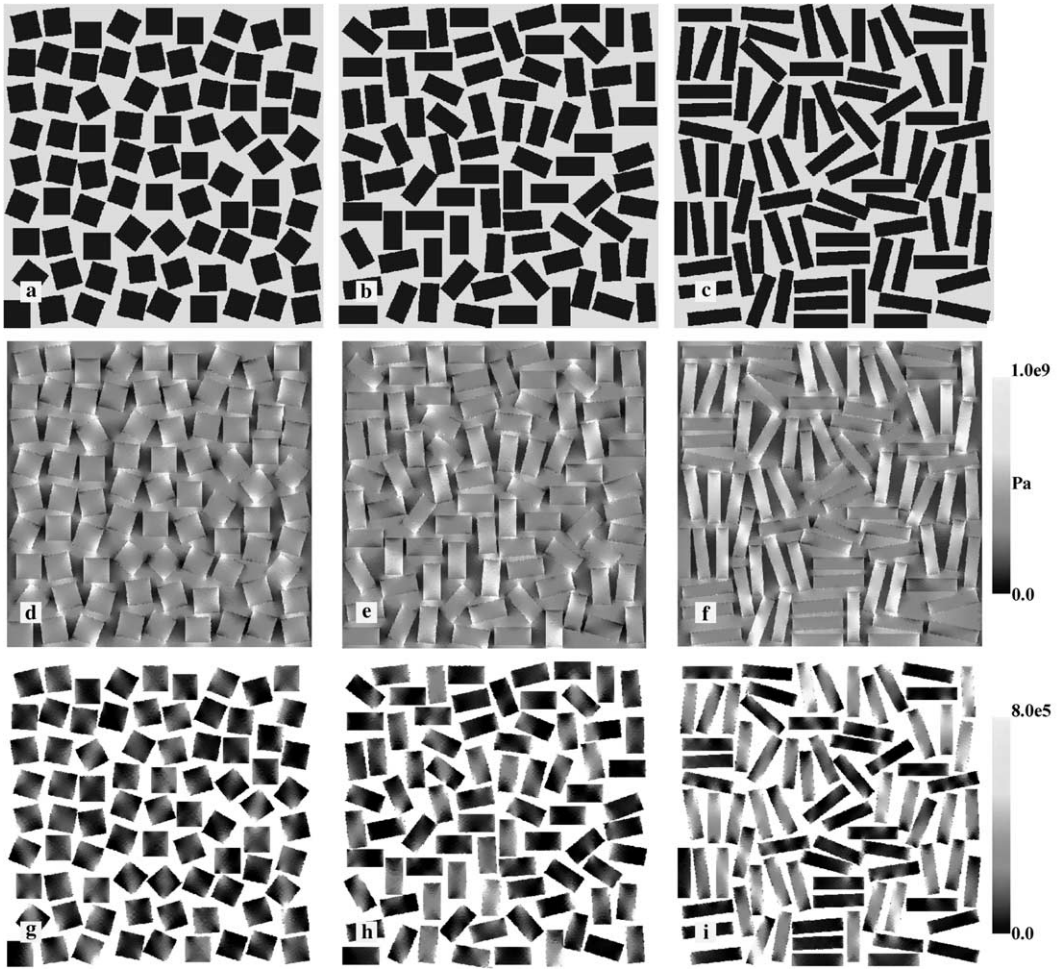

Fig. 11. Examples of hypothetical microstructures (aspect ratio) with their SI1 (Pa) and EED (a.u.) distributions. Simulations performed under a mechanical load alone (0.1% *y*-elongation), fixed and plane-stress boundary conditions. (a) Square microstructure with aspect ratio of 1:1, (b) rectangle microstructure with aspect ratio of 1:2, (c) rectangle microstructure with aspect ratio of 1:4, (d)–(f) SI1 distributions (same scale) and (g)–(i) EED distributions (carbide only, same scale) for (a)–(c) microstructures, respectively.

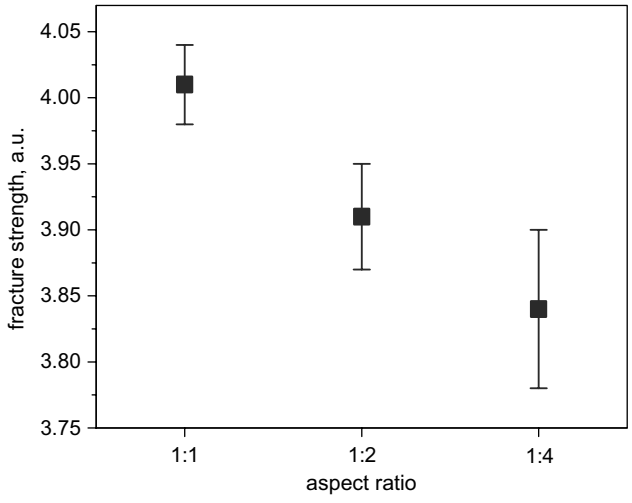

Fig. 12. Plot of the calculated fracture strength (a.u.) with different aspect ratios.

It is important to note that all of the simulations to test the effect of aspect ratio and size distribution were executed with a zero contiguity and a low carbide fraction and this might be thought of as a highly impractical situation. However, it seems likely that the trends revealed by these calculations would be the same. Since the stresses and stored elastic energies are transmitted through the WC skeleton, the effects are likely to be greater in microstructures with higher volume fractions and contiguities. In the future, three-dimensional models will be needed to determine the influence of the connectivity of the carbide network.

6. Conclusions

A brittle fracture model for the fracture strength of WC–Co composites has been developed using a finite

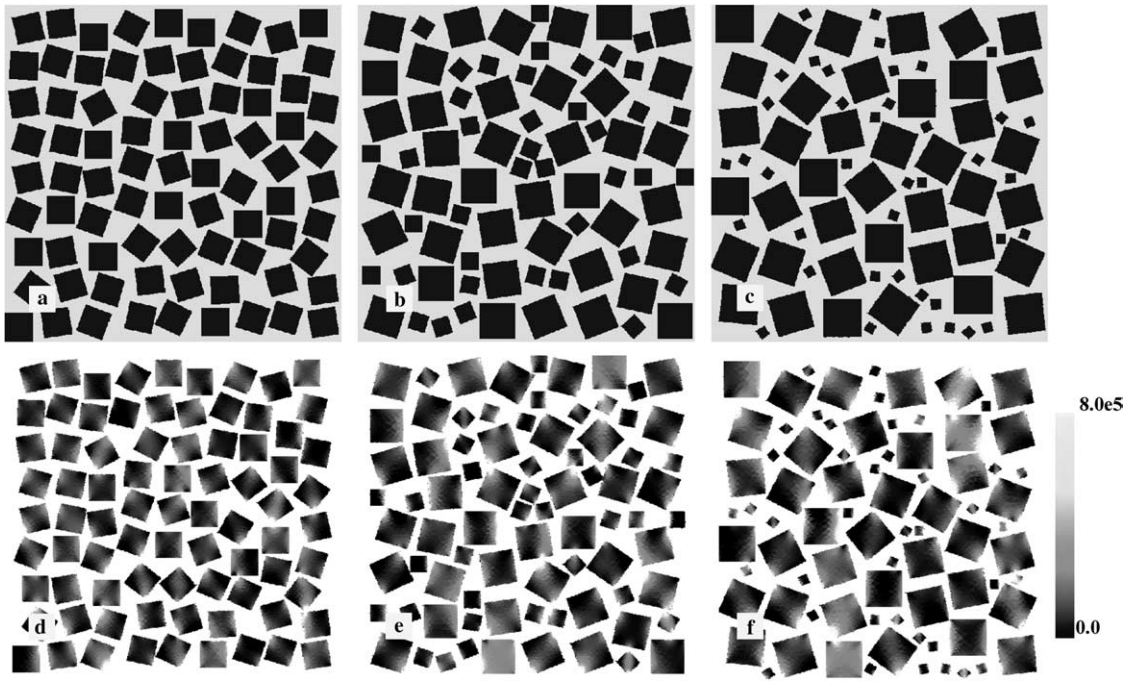

Fig. 13. Examples of hypothetical microstructures (size distribution) with their EED (a.u.) distributions. Simulations performed under a mechanical load alone (0.1% *y*-elongation), fixed and plane-stress boundary conditions. (a) Square microstructure with edge size ratio of 1:1, (b) square microstructure with edge size ratio of 1:2, (c) square microstructure with edge size ratio of 1:4, (d)–(f) EED distributions (carbide only, same scale) for (a)–(c) microstructures, respectively.

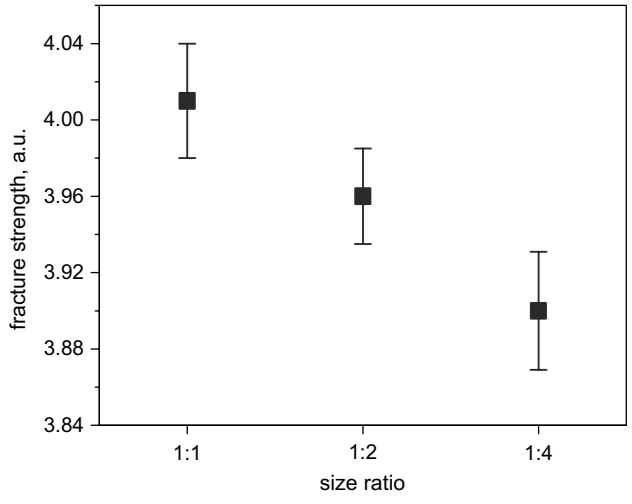

Fig. 14. Plot of the calculated fracture strength (a.u.) with different size ratios.

element analysis. The model assumes that a crack initiates in the brittle carbide phase and that the fracture strength is proportional to the yield strength. When a constant effective surface energy of 49 J/m^2 is used for the fracture criterion under a combined thermal and mechanical load, the sample fails at a strength that approximates the measured transverse rupture strength. This model was then used to calculate the strength of hypothetical microstructures in which selected microstructural characteristics were systematically varied. The most important factor appears to be the connectivity (contiguity) of the carbide skeleton. The angularity, the crystal size distribution, and the aspect ratio of the WC also influence strength, but these parameters are subordinate to contiguity. In summary, the calculations indicate that composites with minimum contiguity, containing highly angular, and equiaxed carbide grains with a narrow size distribution should have the maximum strength.

Acknowledgements

This work was supported primarily by Kennametal Incorporated and the Pennsylvania Technology Infrastructure Authority. Partial support by the MRSEC program of the National Science Foundation under Award Number DMR-0079996 is also acknowledged. We thank A.D. Rollett, Carnegie Mellon University for the image of the W–Ni–Fe alloy.

References

[1] Gurland J. New scientific approaches to development of tool materials. Int Mater Rev 1988;33:151–66.
[2] Exner HE. Physical and chemical nature of cemented carbides. Int Metal Rev 1979;4:149–73.
[3] Roebuck B, Bennett EG. Phase size distribution in WC/Co hard metal. Metallography 1986;19:27–47.

[4] Kim C-S. Microstructural–mechanical property relationships in WC–Co composites. Ph.D. thesis, Carnegie Mellon University, 2004.
[5] Vedula VR, Glass SJ, Saylor DM, Rohrer GS, Carter WC, Langer SA, et al. Residual-stress predictions in polycrystalline alumina. J Am Ceram Soc 2001;84:2947–54.
[6] Chawla N, Patel BV, Koopman M, Chawla KK, Saha R, Patterson BR, et al. Microstructure-based simulation of thermo-mechanical behavior of composite materials by object-oriented finite element analysis. Mater Charact 2003;49:395–407.
[7] Carter WC, Langer SA, Fuller Jr ER, The OOF Manual, version 1.0.8.6, National Institute of Standards and Technology (NIST), 2001, also available online at http://www.ctcms.nist.gov/oof.
[8] Fischmeister HF, Schmauder S, Sigl LS. Finite element modeling of crack propagation in WC–Co hard metals. Mater Sci Eng A 1988;105/106:305–11.
[9] Spiegler R, Fischmeister HF. Prediction of crack paths in WC–Co alloys. Acta Metall Mater 1992;40:1653–61.
[10] Kim C-S, Rohrer GS. Geometric and crystallographic characterization of WC surfaces and grain boundaries in WC–Co composites. Interface Sci 2004;12:19–27.
[11] Lee M, Gilmore RS. Single crystal elastic constants of tungsten monocarbide. J Mater Sci 1982;17:2657–60.
[12] Kelly A, Groves GW. Crystallography and crystal defects. London: Longman; 1973.
[13] Stoll WM, Santhanam AT. Kirk-Othmer encyclopedia of chemical technology. 4th ed. John Wiley and Sons; 1992. p. 861.
[14] Sigl LS, Exner HE. Experimental study of mechanics of fracture in WC–Co alloys. Metall Trans A 1987;18A:1299–308.
[15] Sigl LS, Fischmeister HF. On the fracture toughness of cemented carbides. Acta Metall 1988;36:887–97.